Journal of Energy Storage 152 (2026) 120607

Contents lists available at ScienceDirect

Journal of Energy Storage

journal homepage: www.elsevier.com/locate/est

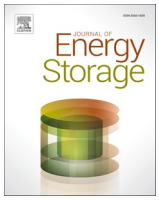

Research Papers

An organic and inorganic composite binder with excellent mechanical property and good ionic conductivity for high performance Si anode of lithium-ion batteries

Lanying He [a], Lixiang Li [a,*], Shuai Wu [a], Fang Di [a,*], Hongwei Zhao [a], Guangshen Jiang [a], Chengguo Sun [a,b], Baigang An [a,*]

[a] Key Laboratory of Energy Materials and Electrochemistry Research Liaoning Province, School of Chemical Engineering, University of Science and Technology Liaoning, 185 Qianshanzhong Road, Anshan, 114051, China
[b] School of Chemical Engineering, Nanjing University of Science and Technology, Nanjing, 210094, China

ARTICLE INFO

Keywords:
Lithium-ion battery
Silicon anode
Binder
Mechanical stability
Li-ion transport

ABSTRACT

The theoretical capacity of silicon (Si) is high, which makes it a highly promising anode material for the development of next-generation lithium-ion batteries (LIBs). However, its severe volume variation (>300%) during lithiation/de-lithiation leads to rapid electrochemical failure, impeding its practical deployment. Addressing this challenge, the optimization of binders emerges as a pivotal strategy. Herein, we developed a composite binder, denoted as CCL, by chemically crosslinking carboxymethyl cellulose (CMC) with lithium silicate (LS) using citric acid (CA). This molecular design integrates the rigidity of LS with the flexibility of CMC, yielding a binder with superior mechanical robustness to accommodate the cyclic strain of Si particles. Furthermore, the CCL binder exhibits strong adhesion to the Si surface through interactions between the Si—O groups in CCL and the silanol (Si-OH) groups on Si. This coupled with the excellent film-forming ability of CMC, ensures electrode integrity. Concurrently, oxygen ions derived from LS enhance lithium-ion transport, thereby improving rate capability. The CCL binder also contributes to a more stable solid electrolyte interphase (SEI) by mitigating parasitic reactions. As a result, the Si/CCL anode delivered exceptional long-term cycling stability, retaining a high reversible capacity of 1192 mAh g^{-1} after 500 cycles at 2.0 A g^{-1}. The superior mechanical and ionic transport properties of CCL also proved advantageous in all-solid-state LIBs, where the anode demonstrated a discharge capacity of 1617.4 mAh g^{-1} at 1.0 A g^{-1} after 100 cycles at 25 °C. These findings underscore the significant potential of the CCL binder for practical Si anodes and offer a valuable design strategy for future binder systems.

1. Introduction

Lithium-ion batteries (LIBs) serve as a key enabling technology for a wide array of applications, including portable electronics, grid-scale energy storage, and electric vehicles, which is attributed to their compelling combination of high energy density, exceptional cycle life, and low self-discharge rate [1–4]. Nevertheless, the low theoretical capacity of graphite anodes poses a significant constraint on achieving higher energy densities in LIBs [5]. In this context, silicon (Si) has garnered considerable attention as a promising alternative, owing to its combination of an ultrahigh theoretical capacity (3579 mAh g^{-1}), a suitable operating voltage (<0.4 V vs. Li^+/Li), and natural abundance [5,6]. However, this pronounced swelling induces severe mechanical fracture of the electrode, thereby inducing continual rupture and reformation of the solid electrolyte interphase (SEI) [7,8]. This has a significant impact on the application of Si anodes in LIBs. A variety of routes have been designed and developed to solve these obstacles, including nano-size and nanostructure of Si, composite structure of Si with carbon materials and functional binders [9–13]. The binders act as a medium to adheres Si active particles together on the current collector and direct contact with electrolyte. Therefore, binders could be designed to meet demands that buffer volumetric stress, supply electronic conductivity, integrate the active particles to adhere the current collector, or stabilize the solid electrolyte film [14–17].

* Corresponding authors.
E-mail addresses: lxli2005@126.com (L. Li), ddifang@163.com (F. Di), baigang73@126.com (B. An).

https://doi.org/10.1016/j.est.2026.120607
Received 24 October 2025; Received in revised form 25 December 2025; Accepted 13 January 2026
Available online 29 January 2026

Polyvinylidene fluoride (PVDF) is a highly prevalent binder in LIBs due to its favourable electrochemical stability and minimal financial expense. However, weak van der Waals interactions between PVDF, Si particles and the current collector, result in poor adhesion strength and severe electrode deformation [18]. The dissolution of PVDF in organic solvents such as *N*-methyl-2-pyrrolidone (NMP), which are toxic, flammable and volatile, is a prerequisite for its use. This renders the electrode preparation process environmentally unfriendly and unsafe. A plethora of water-soluble binders, encompassing polyacrylic acid (PAA), sodium carboxymethyl cellulose (CMC) [19], sodium alginate and gelatin, have been extensively developed. The formation of hydrogen bonds with the abundant Si-OH groups on Si particle surfaces is facilitated by the numerous polar functional groups in these polymers, such as carboxyl, hydroxyl, and amino groups. However, linear structure of these binders proves inadequate in meeting the requirements of Si-based electrodes for long-term cycling stability, fast charging and discharging capabilities, and high initial coulombic efficiency (ICE) [16,20]. A binder with complex interconnected structure by connecting unilinear polymer has better ability to withstand the enormous stress and strain caused by the volume expansion of the Si anode. For instance, Li et al. developed a hard-soft-structured trifunctional network binder (nitrogen-phosphorus-lithium polymer network, N-P-LiPN) that synergistically improves the ionic conductivity of Si-based anodes via a partial lithiation process, simultaneously enhancing the mechanical robustness and adhesion strength of the binder through hydrogen bonding interactions. Shen et al. designed a taurine-grafted polyacrylic acid (Tau-g-PAA) binder. The strong covalent bonds and mechanical interlocking formed by sulfonic acid groups and carboxyl groups in Tau-g-PAA promote multidimensional interactions with Si nanoparticles and lithium-ion diffusion, thereby significantly enhancing the stability and rate performance of Si anodes [21–23]. Chro et al. synthesized a three-dimensionally crosslinked polyacrylic acid/carboxymethyl cellulose (PAA/CMC) composite binder via a dehydration condensation reaction. Due to the cross-linked network formed by CMC and PAA, the mechanical properties of the binder network are optimized, which significantly improves the electrochemical performance of the Si anode [24]. The modification of polymer structures enhances the binder's mechanical robustness by incorporating a crosslinking network, which forms a hard phase capable of alleviating the volume expansion of Si during the lithiation process. However, excessive cross-linking slows down the movement of polymer chains, leading to kinetic hysteresis [25], which has been shown to reduce flexibility and impede ion transport pathways, ultimately limiting the application of Si-based electrodes in fast charging and discharging scenarios.

In recent years, inorganic binders have attracted widespread attentions due to lithium-ion transport ability, including silicates, borates, phosphates, etc. These binders involve the construction of three-dimensional network structures through covalent bonds, ionic bonds, and coordination bonds to promote ion transport. Wang et al. investigated the potential of enhancing lithium-ion transport kinetics by using Lithium silicate (LS), sodium polyphosphate $(NaPO_3)_n$, and lithium monobasic phosphate (LiH_2PO_4) as inorganic binders for Si-based and graphite anodes in LIBs [26]. Among them, LS binders have attracted widespread attention since the oxygen anions on the LS chain can serve as channels for lithium-ion migration [23,27] to improve lithium-ion transport capacity of binder (Fig. S1). However, several critical challenges hinder the application of inorganic binders in Si-based anodes, including high rigidity, brittleness, and insufficient dispersibility [26,28].

The poor flexibility of LS molecular chain makes it difficult to form a continuous and uniform film around Si anodes. In contrast, organic linear binder of CMC owns good film-forming property, but only weak hydrogen bonding is detrimental to the interface stability of Si. Herein, a lightly cross-linked binder (CCL) was designed by grafting small molecule LS onto the chain end of CMC by using CA as a cross-linked agent. CCL binders combine the flexibility and viscoelasticity of organic polymer binders, thereby providing elastic cushioning and adhesion. In addition, it exhibits the rigidity characteristic of inorganic polymer binders, thereby providing enhanced mechanical strength. Furthermore, the oxygen containing anions of LS chain improves the ionic conductivity of Si anodes. The Si electrode with the CCL binder exhibits excellent electrochemical performance, delivering a reversible capacity of 1192 mAh g^{-1} after 100 cycles at 2.0 A g^{-1} and, notably, maintaining 1101 mAh g^{-1} at an ultra-high current density of 6.0 A g^{-1}. Additionally, the Si||NCM811 full cell achieves high energy density, with a capacity retention of 97% under normal operating conditions. The Si electrode incorporating the CCL binder also achieves a high capacity of 1617.4 mAh g^{-1} after 100 cycles at 1.0 A g^{-1} in a solid-state configuration with a PVDF electrolyte, a performance attributable to the efficient ion transport capability of CCL.

2. Experiment

2.1. Materials

Si powders with an average particle size of 30 nm were obtained from Macklin. Citric acid and Lithium silicate solution (Li_2SiO_3, LS, approximately 22 wt%, pH ≈ 12), a precursor solution containing lithium oxide and SiO_2 in a molar ratio of 1:4.8, was procured from Shanghai Aladdin Biochemical Technology Co., Ltd. Carboxymethyl cellulose (CMC), and Super P, a conductive additive, were purchased from Hefei Kejing Material Technology Co., Ltd. All chemicals were used directly without further purification to ensure the consistency and reproducibility of the experiments.

2.2. Material preparation

Initially, CA (5.0 mg) and sodium CMC (9.0 mg) were dissolved in deionized water (1 mL) under magnetic stirring (500 rpm) at ambient temperature (25 ± 1 °C). LS (30.0 mg) was then introduced dropwise into the homogeneous mixture (initial pH of 5.6), The mixture was subsequently subjected to continuous mechanical agitation (800 rpm) for 1 h at 25 ± 1 °C to facilitate ionic complexation and possible esterification between CA and CMC. The resulting organic-inorganic composite binder solution was labeled as CCL. CMC (10 mg) and LS (30.0 mg) were dissolved in deionized water (1 mL) at 25 ± 1 °C using magnetic stirring (500 rpm), and the resulting uniform and stable binder solution was denoted as CL. CMC (20 mg) was dissolved in deionized water (1 mL) at 25 ± 1 °C under magnetic stirring (500 rpm). The resulting uniform and stable binder solution was labeled as CMC. The binder prepared from LS solution is denoted as LS, with the preparation process identical to that of the CMC binder. For electrode fabrication, Si NPs with size of about 30 nm were combined with conductive carbon (Super P, 20 wt%) and CCL binder (20 wt%), according to the optimized mass ratio of 6:2:2. The resulting slurry was doctor-bladed onto copper foil (12 μm thickness) with precise mass loading control (0.82 ± 0.03 mg cm^{-2}). A primary drying at 80 °C for 12 h under vacuum (10 kPa) for solvent evaporation, followed by thermal annealing at 100 °C for 6 h to induce and finish the crosslinking reaction. The process for preparing electrodes using other binders was identical to the method described above. The preparation procedure is illustrated in Fig. S2.

2.3. Material characterization

The morphology of the electrodes, including surface and cross-sectional views, was characterized by scanning electron microscopy (SEM, Thermofisher Apreos), while the sample microstructure was further analyzed by transmission electron microscopy (TEM, Tecnai G2 F20 S-TWIN). The thermal properties of the composite binder, including its glass transition temperature and thermal stability, were evaluated using differential scanning calorimetry (DSC, DSC2500) and thermogravimetric analysis (TGA, TA-Q500). The adhesive strength of the binder

was quantified by a 180° peeling test performed on an electronic universal tensile testing machine (CTM-2500).

2.4. Electrochemical test

In the context of the half-cell assembly, the electrolyte was composed of 1.0 M lithium hexafluorophosphate ($LiPF_6$) in a mixture of ethylene carbonate (EC), diethyl carbonate (DEC), and dimethyl carbonate (DMC) at a volume ratio of 1:1:1. half-cells receive 30 μL of electrolyte per cell, whereas quasi-solid-state half-cells contain 5 μL of electrolyte per cell. Lithium foil was utilized as the counter electrode, while a polyethylene was employed as the separator. In order to guarantee a regulated environment, the assembly of the half-cells into CR2025 coin-type cells was undertaken within a glove box, where the levels of H_2O and O_2 were maintained below 0.01 ppm.

The NCM811 cathode was prepared by coating a slurry of NCM811, Super P, and PVDF (8:1:1 by mass) onto an aluminum foil current collector, followed by vacuum drying at 80 °C for 12 h. The Si anode consisted of Si nanoparticles, Super P, and the CCL binder in a mass ratio of 6:2:2. After being cast onto copper foil and vacuum-dried at 80 °C for 12 h, the anodes were assembled into full-cells with an N/P ratio of 1.15. The calculation of this ratio used the following reversible capacities: 210 mAh g^{-1} for NCM811 and 2700 mAh g^{-1} for the Si/CCL anode. All full-cells were configured as CR2025 coin-type devices and incorporated a 1.0 M $LiPF_6$ electrolyte solution in EC/DEC/DMC (1:1:1 by volume). Cell assembly was performed in an argon-filled glove box with H_2O and O_2 concentrations maintained below 0.01 ppm.

The galvanostatic charge-discharge characteristics of the Si half-cell were evaluated by using the LAND CT2001A battery tester over a voltage range of 0.005–1.5 V. Prior to the cycling measurements, the Si half-cells were activated at 0.05C (1.0C = 3579 mA g^{-1}) for three cycles. The NCM811||Si full-cell battery, with a specific capacity of 210 mAh g^{-1}, was activated at 0.05C and subsequently tested at 1.0C within a voltage window of 2.8–4.3 V, in accordance with the study on the performance of NCM811 batteries.

The cyclic voltammetry (CV) profiles were acquired between 0.005 and 1.2 V (CHI 760E workstation). After activating the electrodes over three cycles at 0.1 mV s^{-1}, the Li^+ diffusion coefficients (D_{Li}^+) were determined by applying the Randles–Ševčík equation:

$$I_p = 2.69 \times 10^5\ n^{1.5}\ AD_{Li}{}^{0.5} + \nu^{0.5}\ C_{Li}{}^{+} \quad (1)$$

The ion diffusion coefficient of the electrode (D_{Li}^+ [$cm^2\ s^{-1}$]), the peak current of the anode or cathode (I_p [A]), the number of electrons transferred (n), the electrode surface area (A [cm^2]), the scan rate (ν [V s^{-1}]), and the concentration of Li^+ (C_{Li}^+ [C mol^{-1}]) are all important factors.

3. Results and discussions

As demonstrated in Scheme 1, CMC with single organic linear binders mainly rely on hydrogen bonds to bond with the substrate and cannot withstand the enormous stress caused by the volume change of the Si anode, making them prone to breakage. LS is rigid but has poor molecular chain flexibility, resulting in low adhesion strength. To develop a binder with good mechanical stability and high lithium-ion transport capability for Si anodes, CMC and small molecule LS were bridged by the crosslinker of CA through esterification reactions and ionic bonding to construct an organic-inorganic composite binder (CCL) with a soft-hard network structure. The CCL binders combine the flexibility and viscoelasticity of organic polymer binders, providing elastic cushioning and adhesion. It also has the rigidity of inorganic binders, providing greater mechanical strength. In addition, LS can form Si-O-Si covalent bonds with Si-OH on the surface of the Si particles, significantly improving the interfacial bind with the surface of the Si NPs, thereby to

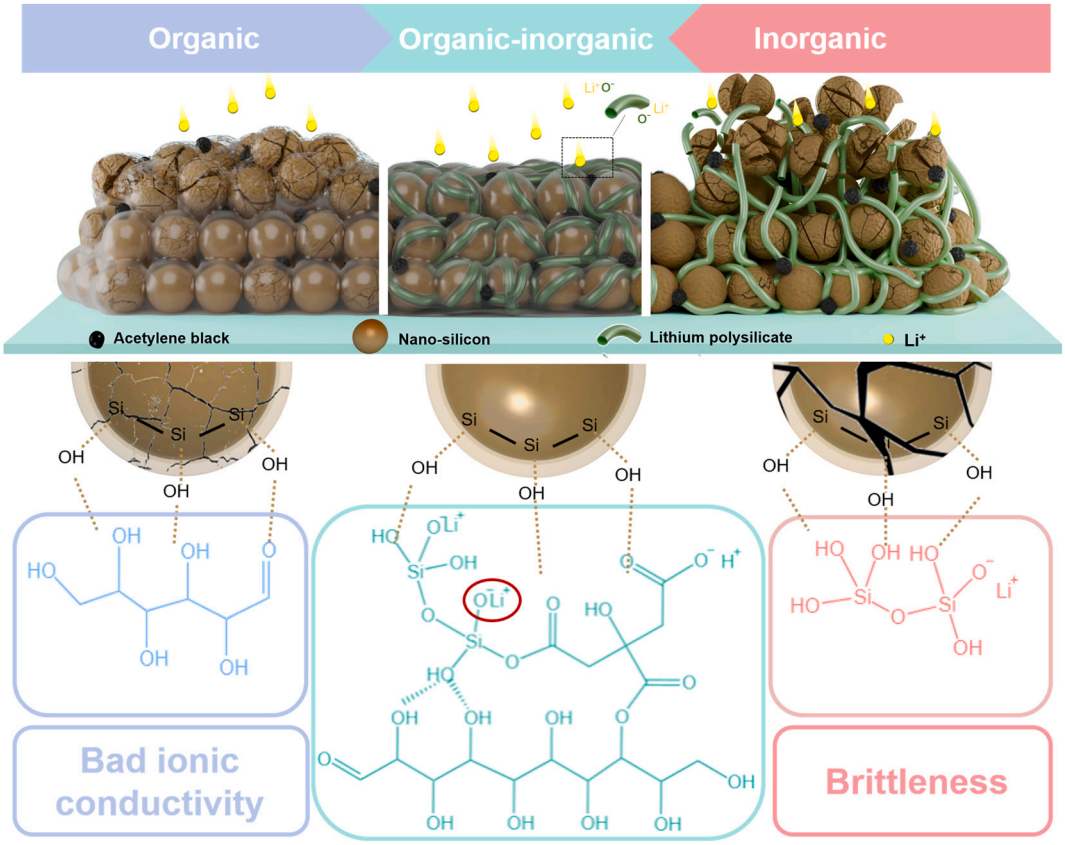

Scheme 1. Schematic diagram of the interaction between CMC, CCL, LS, and Si NPs (from left to right).

maintain the stability of the electrode during cycles. The synergistic movement of oxygen anions in LS provides a fast transmission channel for lithium ions, which helps to achieve efficient ion transport and reduce interface resistance during the cycling process.

To verify the successful grafting of LS onto the terminal chains of CMC, FTIR spectroscopy was conducted on the CCL binders. As shown in Fig. 1a, the peaks observed at 1579 cm^{-1} and 1400 cm^{-1} are attributed to the asymmetric and symmetric stretching vibrations of -COO^- respectively, confirming the presence of CMC [27,29]. The newly emerging peak at 983 cm^{-1} originates from the Si-O-C bond bending vibration formed by the CA-bridged LS, further confirming the successful complexation of CMC with the small-molecule LS via CA [30].

The Si-O-Si stretching vibration at 1236 cm^{-1} in Si NPs exhibits significant broadening in Si/CCL, Si/CL, and Si/LS, further indicating that Si—O groups from the LS component bond with Si-OH groups on the Si NPs surface to form Si-O-Si covalent bonds. Furthermore, the broadening of the Si-O-Si stretching vibration at 1065 cm^{-1} in CCL is attributed to alterations in the local chemical environment arising from the Si-O-C stretching vibration and the stretching vibration of Si-O-Si bonds in amorphous SiO_2 [31–33]. As shown in Fig. S4, high-resolution O 1 s spectroscopy reveals significant alterations in the binding energy and relative abundance of the C—O component within the CCL. Concurrently, a new component attributable to O—Si bonding emerges at approximately 532.5 eV within the O 1 s spectrum. These changes further substantiate the conclusion that LS is linked to CMC via C-O-Si bonds [32]. As shown in Fig. 1b, XRD patterns for both Si and Si/CCL powders revealed characteristic peaks at 28.3°, 47.3°, 56.0°, 69.1°, and 76.4° corresponding to the (111), (220), (311), (400), and (331) crystalline planes of cubic phase Si, indicating that the crystal structure of the Si NPs was not damaged by the CCL network.

Thermal stability of the binders was investigated by thermogravimetric (TG), As shown in Fig. 1d, between the temperatures of 175 °C and 210 °C, the weight of organic polymer binders of CMC and CL decreases significantly, mainly due to the decomposition of organic polymer binders at high temperatures. In contrast, the decomposition of organic-inorganic composite binders of CCL increases to the temperature range of 250 °C to 300 °C. It could be attributed to the thermal barrier effect of inorganic Si—O bonds in the network and the combination of Si—O bonds with carbon chains, which increases the fracture energy barrier and thus improves the stability of the binder. After 300 °C, the TG curve of the LS binder showed a small amount of mass loss, which was due to further dehydration of Si-OH and the ring opening and rearrangement reaction of LS. The weight loss of the CMC and CL binders was due to further thermal cracking after carbonization of the organic polymers. The weight loss of CCL binder after 300 °C includes further dehydration of Si-OH and thermal cracking of organic polymers. The TG of CCL binder tends to be similar to that of organic polymer binder, but its thermal stability is significantly higher than that of CMC and CL binders, indicating that the addition of non-polar components improves the stability of CCL binder. This is extremely beneficial for Si anodes that require long-term stable cycling.

SEM observations of samples are shown in Fig. 1d–g, LS binder is rough and granular, has the poor film-forming properties (Fig. 1e). The CMC binder has good film-forming properties, resulting in the smooth surface (Fig. 1d). The CL binder is composed of granular and flat surfaces, indicating that cross-linking of CMC and LS cannot improve the film-forming properties of the binder. However, CCL binder exhibits a smooth surface covering granular particles, indicating that the network structure of CA cross-linked CMC and LS can provide the binder with good film-forming properties, which could bring the binder good adhesion with Si particles.

The binders should integrate electrode materials through strong adhesion, ensuring mechanical integrity and electrochemical performance in Si-based anodes. To evaluate the adhesion and mechanical stability of the composite binders, the electrodes coated with Si/CL, Si/LS, Si/CMC, and Si/CCL were subjected to a bending test, and their surface morphology was recorded using optical photography (Fig. 2a–d). The results indicate that the Si/CL, Si/LS, and Si/CMC electrodes exhibited significant active material loss after bending, reflecting inadequate binder adhesion and poor structural integrity under mechanical stress. In contrast, the Si/CCL electrode maintained excellent coating integrity even after being bending four times, with only minimal detachment of active material observed. This demonstrates the superior adhesion and mechanical robustness provided by the

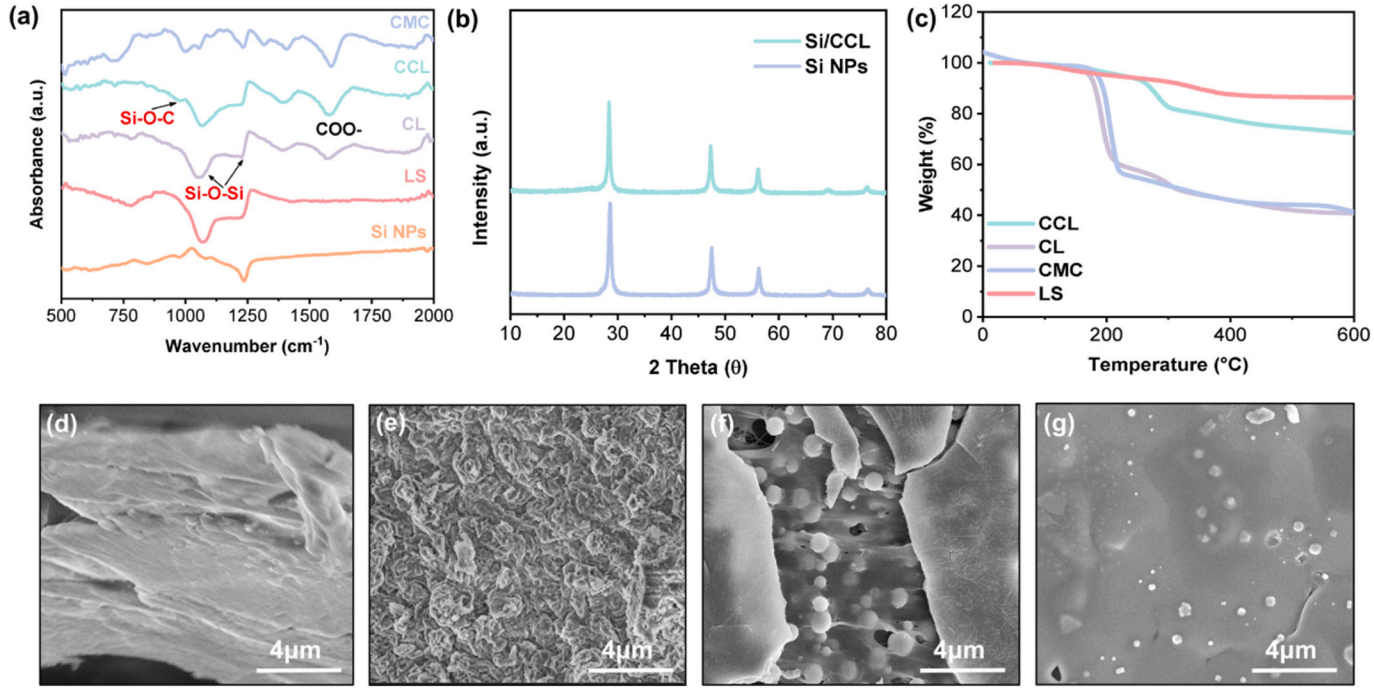

Fig. 1. (a) FTIR spectra of Si/CCL, Si/CL, Si/CMC, and Si/LS; (b) XRD patterns of Si/CCL, Si NPs; (c) TGA curves of CCL, CL, CMC, LS; (d–g) SEM images of corresponding binder films: CMC, LS, CL, and CCL.

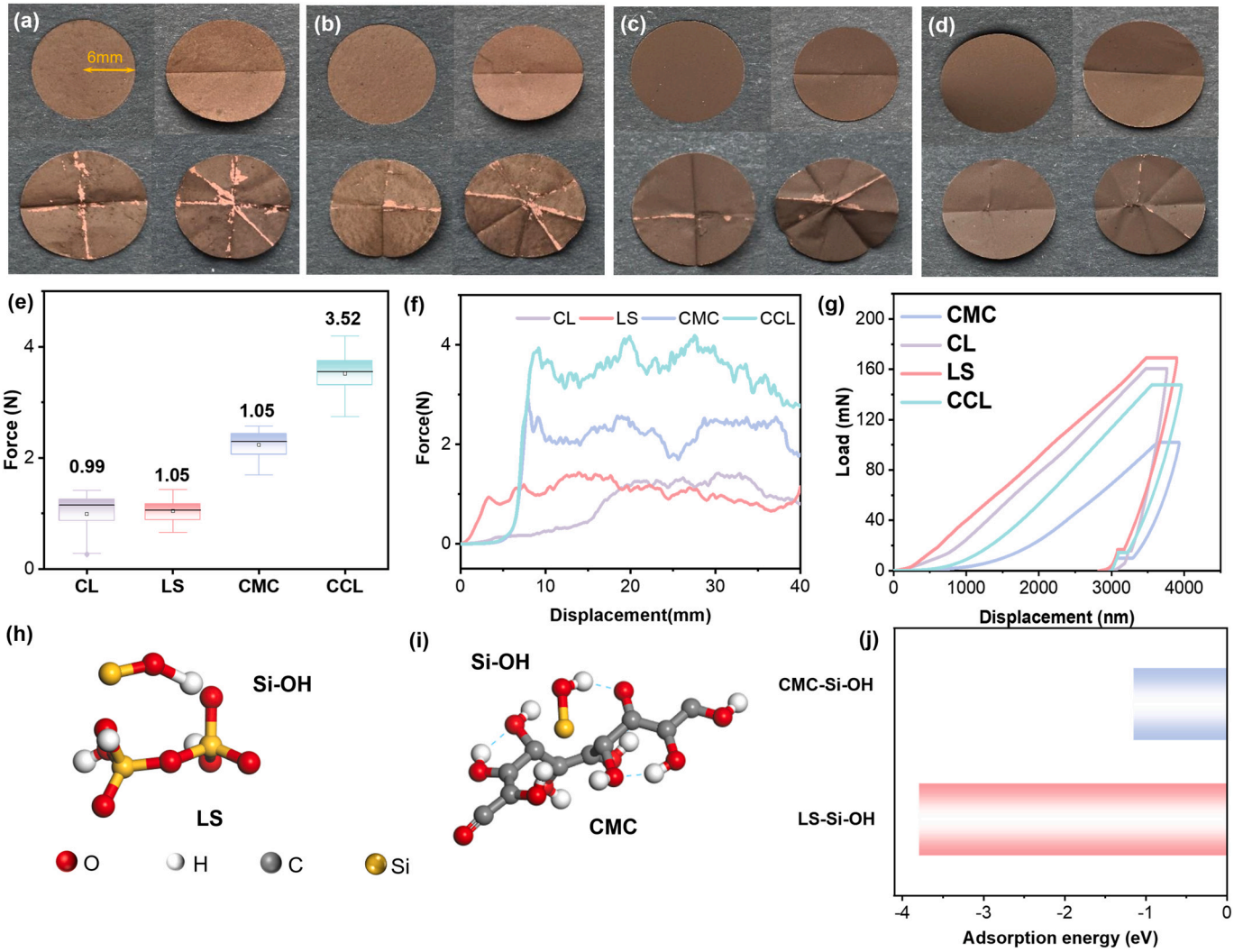

Fig. 2. Mechanical property tests of binders. (a–d) Surface optical images of LS, CL, CMC, and CCL binder electrode by folding tests; (e) statistical analysis of peel strength obtained from the 180° peel test, presented as a box plot of average adhesion force; (f) peel force of Si/CL, Si/LS, Si/CMC, and Si/CCL samples during the 180° peel test; (g) representative load-displacement curve for elastic modulus measurement; LS (h) on Si-OH binding energy, CMC (i) on Si-OH binding energy molecular configuration; (j) the values obtained through molecular simulation calculations.

CCL binder system, which effectively maintains electrode cohesion under repeated deformation. Furthermore, the 180° peel test was conducted and the peel forces of the four binders are summarized in Fig. 2e and f, The CCL binder exhibited the highest peel force against the copper current collector. The average peel force of the CCL binder is 3.52 N, which is even higher as three times as the other three binders (Fig. 2e). The results indicate that CCL binders have better adhesive properties. As the molecular simulation and the theoretical calculation shown in Fig. 2h–j, t the binding energy of LS to Si-OH (−3.7916 eV) is much higher than that of CMC to Si-OH (−1.1466 eV), primarily due to that the strong covalent Si-O-Si bonds between LS and Si, whereas CMC only forms the weak hydrogen bonds with silanol groups. As shown in Fig. S5, the results obtained reveal characteristic peaks at approximately 99.3 eV and 103.4 eV, corresponding to Si^0 and Si^{4+}, respectively. These peaks are primarily attributable to SiO_x/Si-OH groups on the surface of Si NPs. A broadened peak was observed at around 103.6 eV, which corresponds to the Si-O-Si backbone in the LS structure. In the composite sample, the detailed peak fitting identified a novel characteristic peak at approximately 102.8 eV. This binding energy position is distinctly different from the simple superposition of spectral peaks in physical mixtures, lying between typical Si-O-Si and sub-stoichiometric silicon dioxide. This phenomenon is indicative of the formation of Si-O-Si bonds on the silicon surface, a process that occurs through condensation reactions [32].

The Si anodes with good performance require the binder the robust mechanical strength to accommodate the severe volume changes of Si during cycling to maintain electrode integrity. Nanoindentation tests were used to evaluate the mechanical stretchability of the binders. As shown in Fig. 2g, the indentation force of LS is significantly higher than the other three binders at the same indentation depth, suggesting its superior mechanical robustness. The CL and CCL binders prepared by incorporating LS into polymer binders, exhibit the hardness values comparable to the LS binder (Figs. S6 and S7) due to that the addition of LS improves the overall mechanical strength of the binder. Specifically, the elastic modulus of CCL was measured as 12.48 GPa, significantly higher than CMC binders (9.77 GPa). While inorganic binders offer high ionic conductivity and mechanical rigidity, their inherent brittleness limits their effectiveness in accommodating the substantial volumetric changes of silicon anodes. Organic binders, in contrast, provide excellent adhesion and tensile properties, enabling better stress dissipation during cycles. Therefore, we constructed a chemically integrated organic-inorganic composite network. In this system, the inorganic component covalently bonds with the organic matrix. This creates a multi-scale crosslinked structure where the inorganic domains

contribute rigidity, while the organic segments maintain continuous adhesion, elasticity, and cohesion. The synergistic interaction between the phases leads to emergent properties, such as graded modulus and dynamic bond reconfiguration, that are not achievable with either component alone or with a simple physical blend. This integrated network more effectively manages interfacial stress, suppresses crack propagation, and maintains electrical connectivity throughout cycling, addressing the key failure modes of silicon anodes in a complementary manner. The results above demonstrate that the CCL binder owns strong adhesion to both the active material and the current collector, which could supply a Si-based electrode with good cyclability.

Transmission electron microscopy (TEM) was used to observe the microstructure of samples. As shown in Fig. 3a, the Si NPs consist of a crystalline core covered with an amorphous layer. The lattice fringe of crystalline core with the width of 0.31 nm corresponds to the Si (111) crystal plane. The outer amorphous layers ascribe to SiO_x formed by natural oxidation of Si NPs. As shown in Fig. 3b and c, when using CMC as binder, there is a clear interface between the CMC binder layer and the SiO_x layer. However, while CCL binder was applying, such interface cannot be observed. It could be attributed to that the Si—O groups in LS component of CCL bonds with Si-OH on the Si NPs to form the Si-O-Si covalent bonding, the interfacial bonding ability between CCL binder and Si NPs is enhanced.

The corresponded EDS mappings of binder-coated Si NPs are shown in Fig. 3d–k. When CCL is used as a binder, Si and oxygen elements exhibit uniform distribution around Si NPs. Additionally, a dense banded distribution of oxygen elements around Si NPs can be observed, which is attributed to the interaction between oxygen elements in LS molecules and Si—O bonds formed between the CCL binder and Si NPs. In contrast, the particles using CMC as the binder exhibit zones containing elemental oxygen without the presence of Si after cycling. This is attributed to that the CMC binder has no ability to effectively address the volume effect of Si during cycling, leading to fragmentation of the Si NPs.

Wettability of binder plays a critical role in facilitating ion transport and electrochemical reactions within the electrode. As shown in Fig. S8, the contact angles of the binder films with the electrolyte were measured as 28.23°, 24.09°, and 44.29° for CMC, CCL, and LS, respectively. The CCL binder exhibits superior wettability, ensuring efficient electrolyte penetration into the Si/CCL electrode. Furthermore, to guarantee electrode integrity within the electrolyte, swelling tests were conducted. As illustrated in Fig. S9, the Si/CCL electrode exhibited a swelling rate of merely 16.46%, which is much lower than the other electrodes. This indicates that the organic-inorganic composite binder structure can synergistically inhibit excessive electrode swelling and preserving structural integrity.

Si anodes using different binders were used to evaluate the superiority of binders. As cyclic voltammetry (CV) shown in Fig. 4a, the reduction peaks observed between 0.01 V to 0.1 V are attributed to forming Si-lithium alloy phases (such as $Li_{12}Si_7$, $Li_{13}Si_4$, $Li_{17}Si_{13}$, and $Li_{22}Si_{15}$). During de-lithiation, two oxidation peaks appear at 0.38 V and 0.53 V, primarily attributed to the transformation of Si-lithium alloys

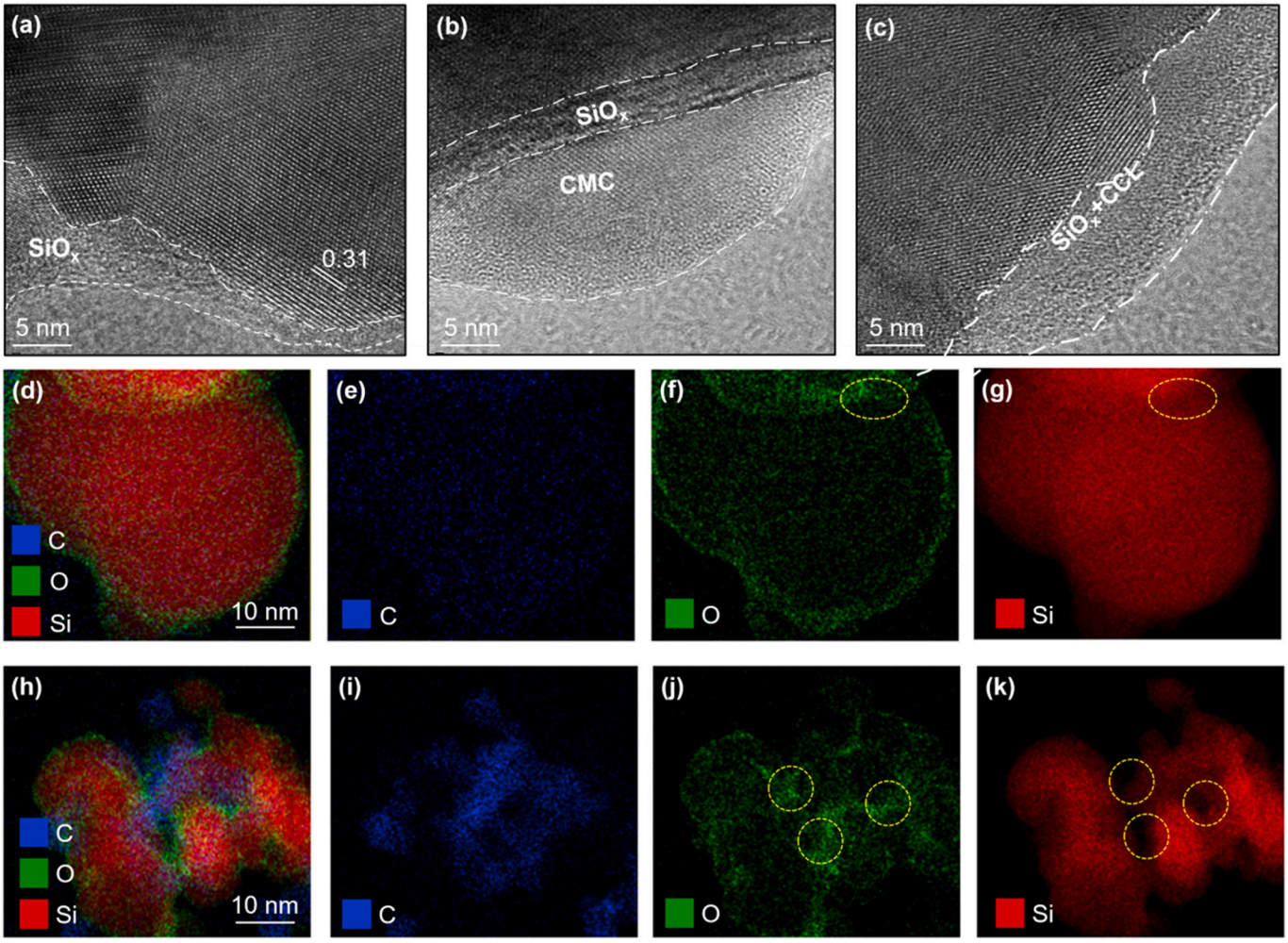

Fig. 3. (a–c) TEM image of Si NPs, CMC binder, and CCL binder-coated Si NPs (mass ratio consistent with half-cell electrode sheet); The corresponding EDS mapping of (d–g) CCL binder binder-coated Si NPs after 100 cycles, and (h–k) CMC binder-coated Si NPs after 100 cycles.

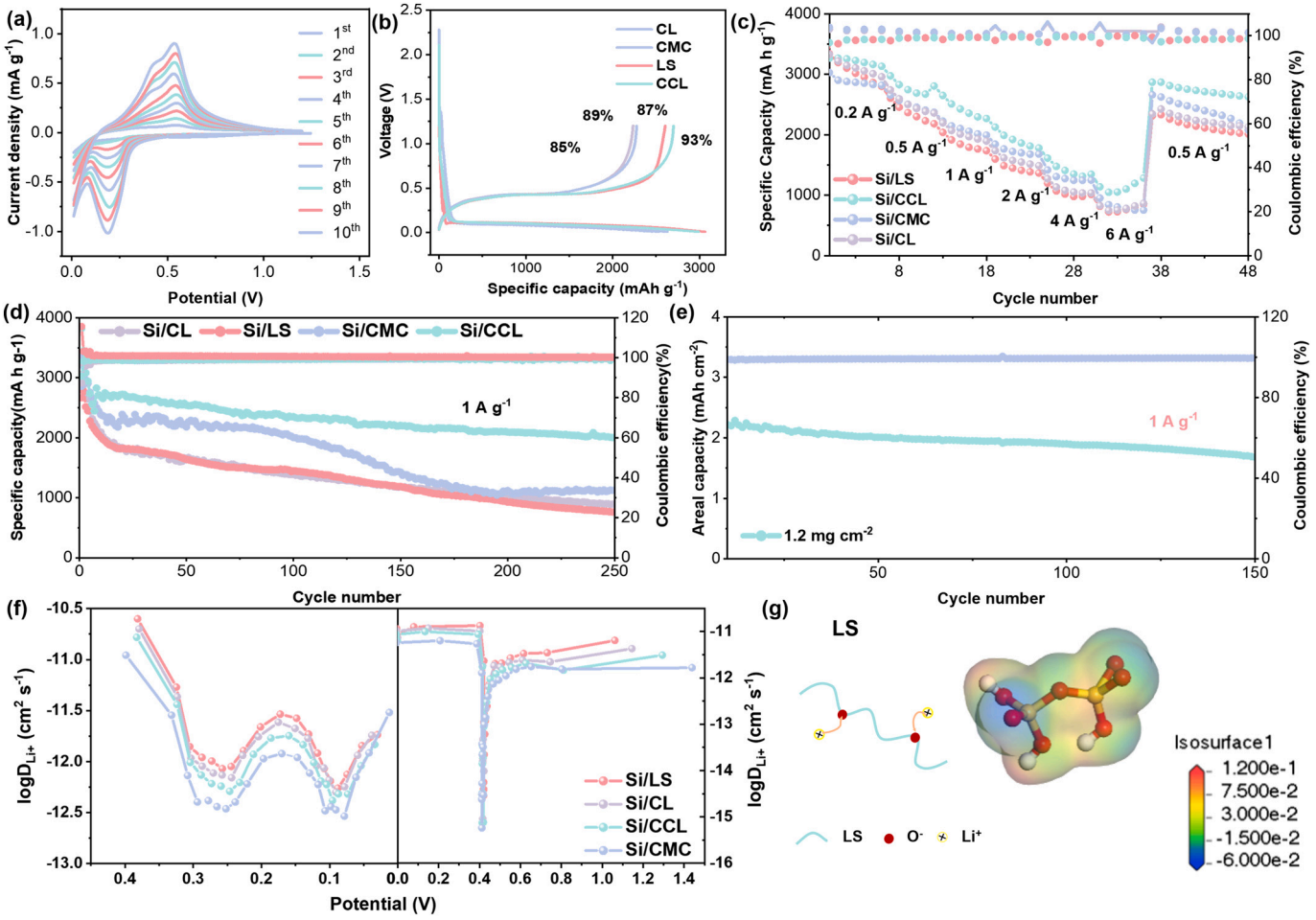

Fig. 4. (a) CV curve of Si/CCL at a scan rate of 0.1 mV s^{-1}; (b) charge and discharge curves of Si anode with binder of CL, CMC, LS and CCL binders at 0.2 A g^{-1}; (c) rate capability assessment at current densities ranging from 0.2 to 5 A g^{-1}; (d) cycling performance of Si electrodes at 1 A g^{-1} over 250 cycles; (e) area capacity of Si/CCL anode with loading of 1.2 mg cm^{-2} at 1.0 A g^{-1}. (f) D_{Li}^{+} of Si anode with binders during the charge/discharge process obtained from the GITT plots; (g) the schematic diagram and electrostatic potential of LS in Density Functional Theory.

(Li_xSi) into amorphous Si during the de-lithiation. As the cycles progress, the peak position remains unchanged, demonstrating the excellent electrochemical stability of Si anode with CCL binder.

As charge-discharge curves shown in Fig. 4b, at the first cycle, the discharge voltage plateau around 0.1 V corresponds to the lithium insertion into crystalline Si to forma Li_xSi_y alloy phase. A charge voltage plateau appears near 0.4 V corresponds to the de-lithiation of Li_xSi_y to transmit into amorphous Si. Compared to the Si anode using the other binders, Si/CCL anode has the best charge-discharge performance with a Coulombic efficiency as high as 93%. Furthermore, the Si/CCL anode demonstrates excellent rate capability (Fig. 4c), delivering the discharge specific capacities of 3227, 2744, 2425.5, 1920.6, 1408.1, and 1101.3 mAh g^{-1} at stepwise current densities of 0.2, 0.5, 1.0, 2.0, 4.0, and 6.0 A g^{-1}, respectively. When the current density was returned to 0.5 A g^{-1}, the capacity recovers to 2776.7 mAh g^{-1}, demonstrating the excellent reversibility of the Si/CCL anode.

Subsequently, we evaluated the cycling stability of Si anodes. As shown in Fig. S10, we systematically investigated adhesives with different mass ratios (CMC:CA:LS of 9:5:6, 9:2:9, and 9:9:2, designated as CCL-5, CCL-2, and CCL-7 respectively). The 9:5:6 ratio exhibited optimal electrochemical properties and was therefore selected as the primary formulation for this study. As shown in Fig. 4d, Si/CCL anode maintains a reversible capacity of 2002.6 mAh g^{-1} at 1.0 A g^{-1} after 250 cycles, accompanying with a capacity retention rate of 73.3%. It delivers a reversible capacity of 1191.4 mAh g^{-1} at 2.0 A g^{-1} after 500 cycles (Fig. S11), get the unit face capacity of 2.33mAh cm^{-2} after 150 cycles at 1.0 A g^{-1}(Fig. 4e). Good long-term cycling stability of Si/CCL anode should be attributed to the improved ionic conductivity and mechanical stability by CCL binder.

To further elucidate the Li^+ diffusion kinetics, the Si/CCL electrode was characterized by galvanostatic intermittent titration technique (GITT). The diffusion coefficients (D_{Li}^{+}) across different charge/discharge states were derived from equation:

$$D_{Li^+} = \frac{4}{\pi\tau}\left(\frac{n_M V_M}{S}\right)^2\left(\frac{\Delta E_S}{\Delta E_\tau}\right)^2 \quad (2)$$

where τ represents the relaxation time (1800 s), n_M and V_M denote the mole number and molar volume of Si, S is the contact area (1.13 cm^2), ΔE_S is the equilibrium potential change over the relaxation period, and ΔE_τ is the potential shift during the galvanostatic pulse. Throughout both the discharge and charge processes, the Si/CCL exhibits the highest Li^+ diffusion coefficient (D_{Li}^{+}) compared to the other electrodes, as illustrated in Fig. 4f. The electrostatic potential of LS was calculated, and the oxygen anion of LS has a more negative potential, indicating a greater attraction to Li^+. This result shows that grafting LS on CMC improves the Li^+ transport capacity of the binder, attributing to the fact that lithium ions can jump through the structural vacancies of O^- in LS to conduct, and the cooperative movement of O^- promotes the rapid transport of lithium ions. This result corresponds to the calculation results of molecular simulation (Fig. 4g).

Cyclic voltammetry (CV) of Si anodes (Fig. S12) further supports the

deduction of LS enhancing ions transport. The peak current of the oxidation peak versus the scanning rates was plotted, the slope fitted by using Randles–Ševčík equation correlates with the kinetic characteristics of Si anode (Fig. S13). A steeper slope indicates faster ion and electron charge transfer rates. As shown in Fig. S13, Si/LS exhibits the highest slope value, further confirming that LS effectively accelerates ion diffusion. Si/CCL also demonstrates a high slope value, significantly exceeding that of Si/CMC. Furthermore, EIS analysis after 100 cycles (Fig. S14) reveals that cells employing Si/CCL retain a lower charge-transfer resistance (Rct) and a higher Li^+ diffusion rate compared to those with Si/CMC, Si/CL, or Si/LS. This indicates that the mechanically robust and resilient organic–inorganic network in CCL effectively mitigates electrode pulverization and maintains interfacial stability during the repeated volume changes, thereby supporting sustained kinetic performance over extended cycles. It demonstrates that grafting LS effectively enhances the ionic conductivity of the binder.

The XPS spectra were charge-corrected using the C 1 s graphite peak at 284.6 eV as an internal reference. As shown in Fig. 5i, the O 1 s energy spectrum exhibits a characteristic peak at 533.6 eV corresponding to oxygen-containing functional groups from C—O— (epoxy/phenol groups) and Si—O bonded structures [34–36]. Notably, the resolved peak at 532.67 eV indicates the presence of carbonyl (C=O) compounds, which can be attributed to the electrochemical decomposition of the carbonate-based electrolyte to form $Li_2CO_3^-$, a characteristic component of the SEI layer in Si-based anodes [37]. The CO_3^{2-} signal intensity of Si/CCL is significantly lower than Si anodes with the other binders, indicating that using CCL binder can effective suppression of electrolyte decomposition. Complementary F 1 s spectra analysis (Fig. 5j) confirms the coexistence of LiF (684.30 eV) and $Li_xPF_yO_z$ species (685.68 eV), which originate from the decomposition of fluorinated electrolyte additives (FEC) and $LiPF_6$ [38,39]. Compared to Si/CMC and Si/CL electrodes, Si/CCL results more LiF in the SEI layer. This LiF-dominated SEI architecture is known to enhance interfacial ionic conductivity while suppressing electron tunneling, thereby improving SEI stability during repeated lithiation/de-lithiation cycles [40]. LS component in CCL can stabilize the SEI layer through Si—O bonds, and suppress the hydrolysis of $LiPF_6$ to produce hydrogen fluoride (HF), thereby effectively scavenging corrosive species. Moreover, the decrease in the concentration of $Li_xPF_yO_z$ and Li_xPF_y species in the Si/CCL indicates that salt decomposition is effectively suppressed [41].

The surface morphologies of the Si-based anodes before and after cycles were characterized by SEM to evaluate the cyclic stability of Si anode with binders. As shown in Fig. 5a–d, the initial electrode surfaces of Si/CL, Si/CMC, and Si/CCL electrodes were relatively smooth, while Si/LS electrode shows large cracks due to the poor flexibility and film-forming properties of the non-polar binder molecular chains, which causes microcracks during the electrode drying process. After 100 cycles, small microcracks appeared on the Si/CL and Si/CMC electrodes, while large cracks appeared on the Si/LS electrode. However, the Si/CCL maintained its structural integrity, and no cracks were observed. Furthermore, the morphology of cycled electrodes was characterized by transmission electron microscopy. As demonstrated in Fig. S15, the thin and well-ordered SEI film was formed around /Si/CCL electrode after cycling, indicating its relative stability. Conversely, the Si/CMC electrode exhibited an agglomerated, block-like SEI film morphology, attributable to the cumulative effect of continuous SEI layer rupture and

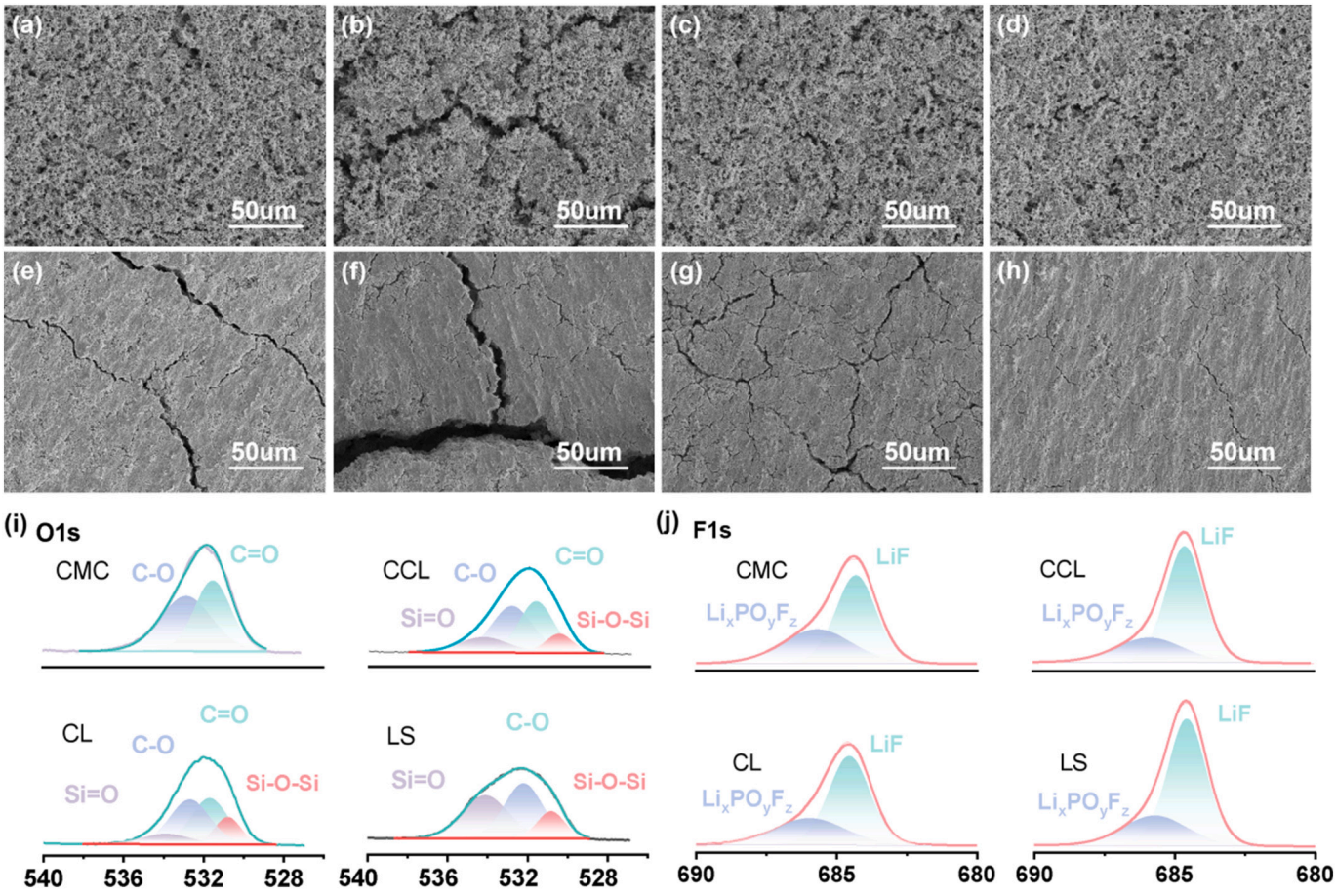

Fig. 5. (a–d) SEM images illustrating the surface morphology of pristine Si electrodes with CL, LS, CMC, and CCL binders; (e–h) comparative SEM analysis of electrode morphology evolution after 100 charge-discharge cycles at 1 A g^{-1}; (i) XPS analysis of O 1s spectra demonstrating the chemical state evolution of surface oxides.; (j) XPS analysis of F 1s spectra, revealing the surface chemical composition after cycling.

regeneration. Furthermore, the fine cracks observed on the surface of the CMC binder indicate that it is incapable of adequately accommodating silicon's volumetric expansion during prolonged cycles. Concurrently, the Si/CL and Si/LS electrodes exhibited only partially discernible particles with a rough, uneven surface, reflecting their inferior stability of the SEI film.

Cross-sectional SEM analysis (Fig. S16) reveal that the thickness expansion ratios of the electrodes after 500 cycles were 215%, 214%, 233%, and 166% for the Si/CL, Si/CMC, Si/LS, and Si/CCL electrodes, respectively, indicating that the CCL binder effectively mitigates volume expansion and mechanical stress during lithiation/de-lithiation. These results show that the organic-inorganic composite binder of CCL constructed by CA cross-linking LS with CMC can handle the huge stress caused by Si volume expansion and keep the electrode components intact during the cycling process.

To validate the practical applicability of the binders on Si based LIBs, a full-cell comprising a Si/CCL anode coupled with a high-nickel $LiNi_{0.8}Co_{0.1}Mn_{0.1}O_2$ (NCM811) cathode, with N/P capacity ratio of 1.15:1 was assembled (Fig. 6a). The full cell can supply a current of up to 189.6 mA at a rate of 1.0C, and has an internal energy efficiency rating of 96.3%. As shown in Fig. 6e, a Si/CCL|NCM811 assembled button cell battery can power commercial LED light strips. As shown in Fig. 6g, comparing with other outstanding works in the same field, it can be found that CCL binder has greater advantages in terms of rate performance, discharge specific capacity, and capacity retention [42–53]. CCL binder contributing to good performance of LIB can be attributed to the aspects as follow. CMC grafted LS greatly improves the mechanical properties and adhesion of the CCL binder, enabling it to better withstand the stress caused by the volume expansion of the Si anode. The lower negative potential of oxygen ions in the LS molecular chain provides binding sites for lithium ions, promoting Li^+ transport capacity and improving rate performance [50].

Base on the good mechanical properties and ion conductivity of CCL, we investigated the possibility of CCL binder used in a quasi-solid-state LIB, in which Si/CCL and lithium metal was used as the anode and cathode, a PVDF-based was used as the solid electrolyte membrane (Fig. 6c). The cycling performance was assessed at a current density of 1.0 A g^{-1} under ambient conditions (25 °C) using galvanostatic charge/discharge measurements. The quasi-solid-state LIB demonstrates a discharge specific capacity of 1617.4 mAh g^{-1} after 100 cycles, corresponding to 67.2% capacity retention (Fig. 6d). As shown in Fig. 6f, the dQ/dV curve of the solid-state battery exhibits peaks at 0.06 V and 0.17 V corresponding to lithiation, while the cathode peaks at 0.32 V and 0.52 V correspond to de-lithiation. As cycling progresses, the peak

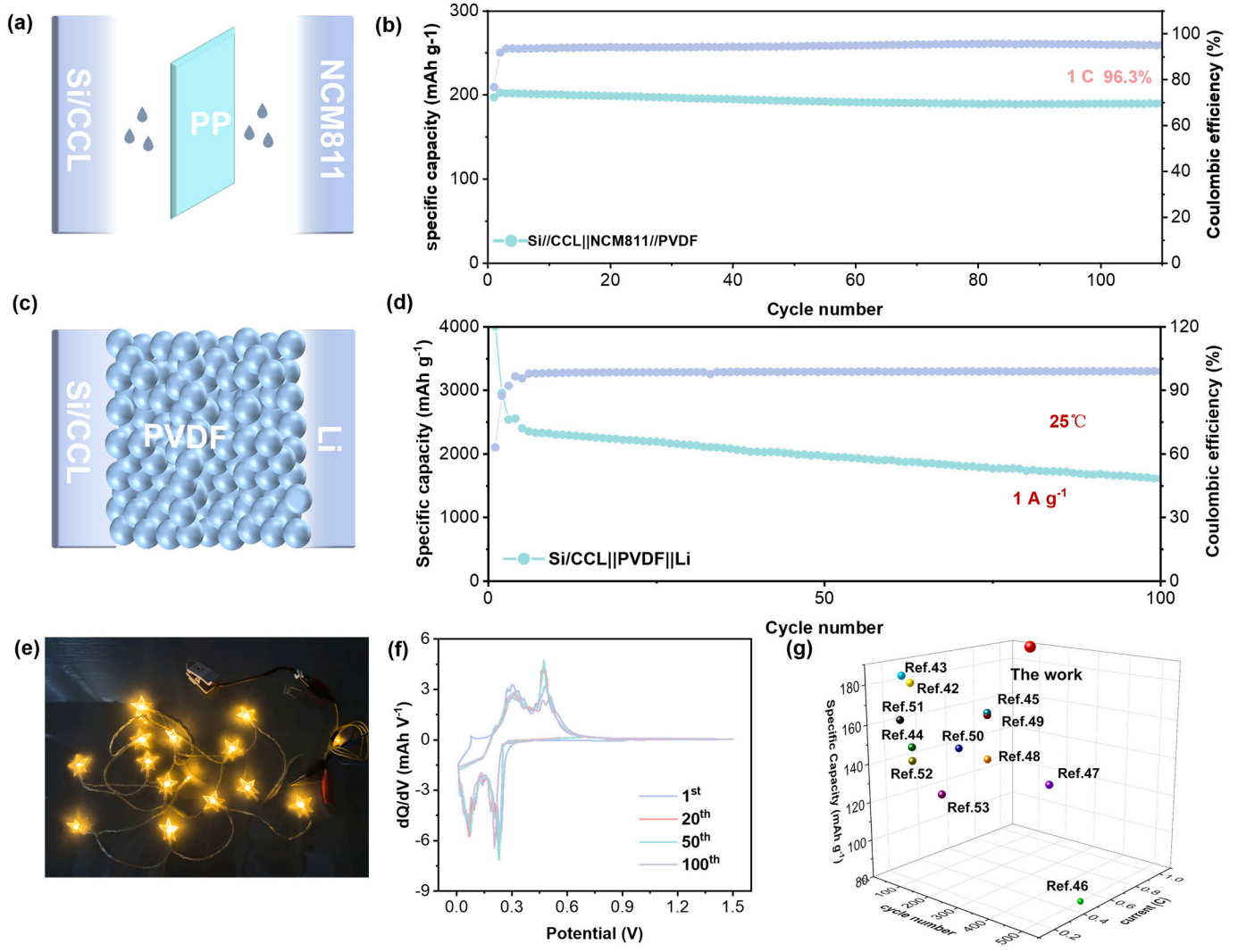

Fig. 6. (a) Schematic diagram of the Si/CCL||NCM811/PVDF full cell; (b) the Si/CCL||NCM811/PVDF full cell at 1C (2.5 mA cm^{-2}) cycling stability; (c) schematic diagram of the Si/CCL||Li solid-state battery; (d) electrochemical performance of the Si/CCL||Li half-cell with PVDF as the solid electrolyte membrane at 1 A g^{-1}; (e) a homemade button battery (CR2032) driving an LED device; (f) dQ/dV of the Si/CCL||Li solid-state battery; (g) performance comparison of Si/CCL||NCM811 full cell with the related publications.

positions remain unchanged, demonstrating the excellent electrochemical stability of the binder in quasi-solid-state batteries.

4. Conclusion

In summary, organic and inorganic composite binder of CCL that owns flexibility, rigidity and ions transport capability adapting to Si anode has been successfully designed and prepared. CCL binder consists of a flexible CMC crosslinked with a rigid LS by using CA as a cross-linking agent through the esterification reactions. Oxygen containing groups from CCL can bond with Si-OH around surface of Si particles to result the strong adhesion between CCL, Si particles and the current to fabricate a robust Si anode. Meanwhile, CCL around Si particle can also promote lithium ions transport due to the lower negative potential of oxygen ions on the LS molecular chain. When evaluated in half-cell configurations, the Si/CCL anode demonstrates exceptional cycling stability, maintaining a specific discharge capacity of 1192 mAh g^{-1} after 500 cycles at a high current density of 2.0 A g^{-1}. In tests where the battery is fully charged and used, the NCM811 cathode works very well. After 110 cycles at 1.0 C rate, the battery retains 96.3% of its initial capacity and has a discharge capacity of 189.8 mAh g^{-1}. Furthermore, good mechanical properties and good ions transport ability make the Si/CCL anode using PVDF as solid electrolyte achieve a discharge specific capacity of 1617.4 mAh g^{-1} at 1.0 A g^{-1} after 100 cycles at 25 °C. This organic-inorganic composite Si-based binder paves the way for next-generation high-energy-density Si anode binders.

CRediT authorship contribution statement

Lanying He: Writing – review & editing, Writing – original draft, Visualization, Validation, Software, Methodology, Formal analysis, Data curation, Conceptualization. **Lixiang Li:** Supervision, Data curation, Formal analysis, Writing – original draft. **Shuai Wu:** Supervision, Validation. **Fang Di:** Data curation, Formal analysis, Software. **Hongwei Zhao:** Data curation, Formal analysis, Investigation. **Guangshen Jiang:** Data curation, Formal analysis. **Chengguo Sun:** Data curation, Formal analysis. **Baigang An:** Writing – review & editing, Supervision, Funding acquisition, Conceptualization, Methodology, Writing – original draft.

Declaration of competing interest

The authors declare that they have no known competing financial interests or personal relationships that could have appeared to influence the work reported in this paper.

Acknowledgments

This work was supported by the NSFC [Grant No. 52371224 and 51972156], University of Science and Technology Liaoning Talent Project [Grant No. 6003000317] and the Basic Research Projects for Higher Education Institutions Liaoning Provincial Education Department [Grant No. LJ212510146018].

Appendix A. Supplementary data

Supplementary data to this article can be found online at https://doi.org/10.1016/j.est.2026.120607.

Data availability

Data will be made available on request.

References

[1] J.B. Goodenough, K.-S. Park, The Li-ion rechargeable battery: a perspective, J. Am. Chem. Soc. 135 (2013) 1167–1176, https://doi.org/10.1021/ja3091438.
[2] A. Bilich, K. Langham, R. Geyer, L. Goyal, J. Hansen, A. Krishnan, J. Bergesen, P. Sinha, Life cycle assessment of solar photovoltaic microgrid systems in off-grid communities, Environ. Sci. Technol. 51 (2016) 1043–1052, https://doi.org/10.1021/acs.est.6b05455.
[3] D. Chen, Z. Lou, K. Jiang, G. Shen, Device configurations and future prospects of flexible/stretchable lithium-ion batteries, Adv. Funct. Mater. 28 (2018) 1805596, https://doi.org/10.1002/adfm.201805596.
[4] C.P. Grey, D.S. Hall, Prospects for lithium-ion batteries and beyond—a 2030 vision, Nat. Commun. 11 (2020) 6279, https://doi.org/10.1038/s41467-020-19991-4.
[5] D. Ma, Z. Cao, A. Hu, Si-based anode materials for Li-ion batteries: a mini review, Nano-Micro Lett. 6 (2014) 347–358, https://doi.org/10.1007/s40820-014-0008-2.
[6] G. Xie, X. Tan, Z. Shi, Y. Peng, Y. Ma, Y. Zhong, F. Wang, J. He, Z. Zhu, X.B. Cheng, G. Wang, T. Wang, Y. Wu, SiO_x based anodes for advanced Li-ion batteries: recent progress and perspectives, Adv. Funct. Mater. 6 (2024) 347–358, https://doi.org/10.1002/adfm.202414714.
[7] S. Chae, M. Ko, K. Kim, K. Ahn, J. Cho, Confronting issues of the practical implementation of Si anode in high-energy lithium-ion batteries, Joule 1 (2017) 47–60, https://doi.org/10.1016/j.joule.2017.07.006.
[8] L. Li, Z. Wang, H. Li, X. Luo, Z. Li, A. Fu, X. Liu, Y. Guo, H. Li, ZIF-67 decorated PVDF fibers embedded in PEO and infiltrated with ionic liquid as composite polymer electrolyte for high performance secondary batteries using lithium metal as anode, J. Energy Storage 124 (2025) 116932, https://doi.org/10.1016/j.est.2025.116932.
[9] Z. Chen, A. Soltani, Y. Chen, Q. Zhang, A. Davoodi, S. Hosseinpour, W. Peukert, W. Liu, Emerging organic surface chemistry for Si anodes in lithium-ion batteries: advances, prospects, and beyond, Adv. Energy Mater. 12 (2022) 2200924, https://doi.org/10.1002/aenm.202200924.
[10] Z. He, L. Liu, S. Liu, Y. Chen, L. Sun, C. Liu, Y. Zhu, X. Wang, A novel design idea of high-stability silicon anodes for lithium-ion batteries: building in-situ "high-speed channels" while reserving space, Chem. Eng. J. 472 (2023) 144991, https://doi.org/10.1016/j.cej.2023.144991.
[11] J.-I. Lee, Y. Ko, M. Shin, H.-K. Song, N.-S. Choi, M.G. Kim, S. Park, High-performance silicon-based multicomponent battery anodes produced via synergistic coupling of multifunctional coating layers, Energ, Environ. Sci. 8 (2015) 2075–2084, https://doi.org/10.1039/C5EE01493J.
[12] D. Cao, T. Ji, A. Singh, S. Bak, Y. Du, X. Xiao, H. Xu, J. Zhu, H. Zhu, Unveiling the mechanical and electrochemical evolution of nanosilicon composite anodes in sulfide-based all-solid-state batteries, Adv. Energy Mater. 13 (2023) 2203969, https://doi.org/10.1002/aenm.202203969.
[13] W. Luo, X. Chen, Y. Xia, M. Chen, L. Wang, Q. Wang, W. Li, J. Yang, Surface and interface engineering of silicon-based anode materials for lithium-ion batteries, Adv. Energy Mater. 7 (2017) 1701083, https://doi.org/10.1002/aenm.201701083.
[14] Z. Yang, C. Wu, S. Li, L. Qiu, Z. Yang, Y. Zhong, B. Zhong, Y. Song, G. Wang, Y. Liu, Z. Wu, X. Guo, A unique structure of highly stable interphase and self-consistent stress distribution radial-gradient porous for silicon anode, Adv. Funct. Mater. 32 (2021) 2107897, https://doi.org/10.1002/adfm.202107897.
[15] H. Chen, M. Ling, L. Hencz, H.Y. Ling, G. Li, Z. Lin, G. Liu, S. Zhang, Exploring chemical, mechanical, and electrical functionalities of binders for advanced energy-storage devices, Chem. Rev. 118 (2018) 8936–8982, https://doi.org/10.1021/acs.chemrev.8b00241.
[16] Q. He, J. Ning, H. Chen, Z. Jiang, J. Wang, D. Chen, C. Zhao, Z. Liu, I.F. Perepichka, H. Meng, W. Huang, Achievements, challenges, and perspectives in the design of polymer binders for advanced lithium-ion batteries, Chem. Soc. Rev. 53 (2024) 7091–7157, https://doi.org/10.1039/D4CS00366G.
[17] T. Wang, Z. Wang, H. Li, L. Cheng, Y. Wu, X. Liu, L. Meng, Y. Zhang, S. Jiang, Recent status, key strategies, and challenging prospects for fast charging silicon-based anodes for lithium-ion batteries, Carbon 230 (2024) 119615, https://doi.org/10.1016/j.carbon.2024.119615.
[18] S. Yu, Y. Liu, C. Ding, X. Liu, Y. Liu, D. Wu, H. Luo, S. Chen, All-organic sandwich structured polymer dielectrics with polyimide and PVDF for high temperature capacitor application, J. Energy Storage 62 (2023) 106868, https://doi.org/10.1016/j.est.2023.106868.
[19] D. Mazouzi, R. Grissa, M. Paris, Z. Karkar, L. Huet, D. Guyomard, L. Roué, T. Devic, B. Lestriez, CMC-citric acid Cu(II) cross-linked binder approach to improve the electrochemical performance of Si-based electrodes, Electrochim. Acta 304 (2019) 495–504, https://doi.org/10.1016/j.electacta.2019.03.026.
[20] J. Liu, Q. Zhang, T. Zhang, J.T. Li, L. Huang, S.G. Sun, A robust ion-conductive biopolymer as a binder for Si anodes of lithium-ion batteries, Adv. Funct. Mater. 25 (2015) 3599–3605, https://doi.org/10.1002/adfm.201500589.
[21] J. Shen, S. Zhang, H. Wang, R. Wang, Y. Hu, Y. Mao, R. Wang, H. Zhang, Y. Du, Y. Fan, Y. Zhou, Z. Guo, B. Wang, Unlocking the potential of silicon anodes in lithium-ion batteries: a claw-inspired binder with synergistic interface bonding, eScience 4 (2024) 100207, https://doi.org/10.1016/j.esci.2023.100207.
[22] L. Zhang, X. Wu, W. Qian, K. Pan, X. Zhang, L. Li, M. Jia, S. Zhang, Exploring more functions in binders for lithium batteries, Electrochem. Energy Rev. 6 (2023) 36, https://doi.org/10.1007/s41918-023-00198-2.
[23] F. Wang, Q. Zhang, Z. Liu, M. Hou, Z. Li, J. Liu, R. Wang, L. Wang, A bifunctional lithium polysilicate as highly efficient adhesion agent and anchoring host for long-lifespan Li-S battery, J. Colloid Interface Sci. 629 (2023) 1045–1054, https://doi.org/10.1016/j.jcis.2022.09.026.
[24] N. Kuganathan, L.H. Tsoukalas, A. Chroneos, Defects, dopants and Li-ion diffusion in Li_2SiO_3, Solid State Ionics 335 (2019) 61–66, https://doi.org/10.1016/j.ssi.2019.02.019.
[25] Y. Su, X. Rong, A. Gao, Y. Liu, J. Li, M. Mao, X. Qi, G. Chai, Q. Zhang, L. Suo, L. Gu, H. Li, X. Huang, L. Chen, B. Liu, Y.-S. Hu, Rational design of a topological

polymeric solid electrolyte for high-performance all-solid-state alkali metal batteries, Nat. Commun. 13 (2022) 4181, https://doi.org/10.1038/s41467-022-31792-5.
[26] C. Wei, M.N. Obrovac, Inorganic compounds as binders for Si-alloy anodes, J. Electrochem. Soc. 168 (2021) 020505, https://doi.org/10.1149/1945-7111/abdc74.
[27] X. Wang, K. Wang, Z. Zheng, Z. Wan, J. Zhao, H. Li, W. Jiang, Z. Wu, B. Chen, Y. Tan, M. Ling, M. Sun, C. Liang, Advanced inorganic lithium metasilicate binder for high-performance silicon anode, J. Colloid Interface Sci. 652 (2023) 971–978, https://doi.org/10.1016/j.jcis.2023.08.071.
[28] J. Zhao, D. Wei, J. Wang, K. Yang, Z. Wang, Z. Chen, S. Zhang, C. Zhang, X. Yang, Inorganic crosslinked supramolecular binder with fast self-healing for high performance silicon based anodes in lithium-ion batteries, J. Colloid Interface Sci. 625 (2022) 373–382, https://doi.org/10.1016/j.jcis.2022.06.002.
[29] R. Song, X. Wang, M. Johnson, C. Milne, A. Lesniak-Podsiadlo, Y. Li, J. Lyu, Z. Li, C. Zhao, L. Yang, I. Lara-Sáez, S. A, W. Wang, Enhanced strength for double network hydrogel adhesive through cohesion-adhesion balance, Adv. Funct. Mater. 34 (2024) 373–382, https://doi.org/10.1002/adfm.202313322.
[30] N.T. Han, V.K. Dien, N.T. Thuy Tran, D.K. Nguyen, W.-P. Su, M.-F. Lin, First-principles studies of electronic properties in lithium metasilicate (Li_2SiO_3), RSC Adv. 10 (2020) 24721–24729, https://doi.org/10.1039/D0RA01583K.
[31] G. Li, W. Cai, B. Liu, Z. Li, A multi functional binder with lithium ion conductive polymer and polysulfide absorbents to improve cycleability of lithium–sulfur batteries, J. Power Sources 294 (2015) 187–192, https://doi.org/10.1016/j.jpowsour.2015.06.083.
[32] M. Zhang, J. Lu, P. Li, X. Li, G. Yuan, Y. Zuo, Construction of high-efficiency fixing structure of waterborne paint on silicate-modified poplar surfaces by bridging with silane coupling agents, Prog. Org. Coat. 167 (2022) 106846, https://doi.org/10.1016/j.porgcoat.2022.106846.
[33] J. Sun, X. Huang, Y. Liu, K. Zhang, Y. Yan, Y. Liu, X. Yan, Enhanced microwave absorption performance originated from interface and unrivaled impedance matching of SiO_2/carbon fiber, Appl. Surf. Sci. 623 (2023) 157029, https://doi.org/10.1016/j.apsusc.2023.157029.
[34] J. Liu, Q. Zhang, Y.-K. Sun, Recent progress of advanced binders for Li-S batteries, J. Power Sources 396 (2018) 19–32, https://doi.org/10.1016/j.jpowsour.2018.05.096.
[35] Y. Lin, J. Jiang, Y. Zhang, X. He, J. Ren, P. He, C. Pang, C. Xiao, D. Yang, N. Du, Promoting effect of Si–OH on the decomposition of electrolytes in lithium-ion batteries, Chem. Mater. 32 (2020) 6365–6373, https://doi.org/10.1021/acs.chemmater.0c01022.
[36] Z. Luo, Y. Xu, C.-R. Gong, Y.-Q. Zheng, Z.-X. Zhou, L.-M. Yu, An ultraviolet curable silicon/graphite electrode binder for long-cycling lithium ion batteries, J. Power Sources 485 (2021) 229348, https://doi.org/10.1016/j.jpowsour.2020.229348.
[37] S.B. Son, L. Cao, T. Yoon, A. Cresce, S.E. Hafner, J. Liu, M. Groner, K. Xu, C. Ban, Interfacially induced cascading failure in graphite-silicon composite anodes, Adv. Sci. 6 (2018) 1801007, https://doi.org/10.1002/advs.201801007.
[38] H. Shin, J. Park, A.M. Sastry, W. Lu, Effects of fluoroethylene carbonate (FEC) on anode and cathode interfaces at elevated temperatures, J. Electrochem. Soc. 162 (2015) A1683–A1692, https://doi.org/10.1149/2.0071509jes.
[39] Z. Cao, X. Zheng, W. Huang, Y. Wang, Q. Qu, H. Zheng, Dynamic bonded supramolecular binder enables high-performance silicon anodes in lithium-ion batteries, J. Power Sources 463 (2020) 228208, https://doi.org/10.1016/j.jpowsour.2020.228208.
[40] H. Jin, S. Pyo, H. Seo, J. Cho, J. Han, J. Han, H. Yun, H. Kim, J. Lee, B. Min, J. Yoo, Y.S. Kim, LiF-rich solid electrolyte interphase formation by establishing sacrificial layer on the separator, Small (2024) 2401928, https://doi.org/10.1002/smll.202401928.
[41] D. Aurbach, Review of selected electrode–solution interactions which determine the performance of Li and Li ion batteries, J. Power Sources 89 (2000) 206–218, https://doi.org/10.1016/S0378-7753(00)00431-6.
[42] Y. Wang, N. Dong, B. Liu, G. Tian, S. Qi, D. Wu, Self-adaptive gel poly (imide-siloxane) binder ensuring stable cathode-electrolyte interface for achieving high-performance NCM811 cathode in lithium-ion batteries, Energy Storage Mater. 56 (2023) 621–630, https://doi.org/10.1016/j.ensm.2023.02.002.
[43] X. Li, W. Liu, Y. Wang, L. Lv, H. Feng, S. Gu, H. Zheng, Decorating silicon surface by an electroactive covalent organic framework to develop high-performance lithium-ion batteries, Energy Storage Mater. 66 (2024) 103207, https://doi.org/10.1016/j.ensm.2024.103207.
[44] Y. Dong, B. Zhang, F. Zhao, F. Gao, D. Liu, Dendrimer based binders enable stable operation of silicon microparticle anodes in lithium-ion batteries, Small 19 (2023) 2206858, https://doi.org/10.1002/smll.202206858.
[45] D.Y. Han, I.K. Han, H.B. Son, Y.S. Kim, J. Ryu, S. Park, Layering charged polymers enable highly integrated high-capacity battery anodes, Adv. Funct. Mater. 33 (2023) 2213458, https://doi.org/10.1002/adfm.202213458.
[46] W. Cao, J. Lu, K. Zhou, G. Sun, J. Zheng, Z. Geng, H. Li, Organic-inorganic composite SEI for a stable Li metal anode by in-situ polymerization, Nano Energy 95 (2022) 106983, https://doi.org/10.1016/j.nanoen.2022.106983.
[47] C. Sun, H. Zhang, P. Mu, G. Wang, C. Luo, X. Zhang, C. Gao, X. Zhou, G. Cui, Covalently cross-linked chemistry of a three-dimensional network binder at limited dosage enables practical Si/C composite electrode applications, ACS Nano 18 (2024) 2475–2484, https://doi.org/10.1021/acsnano.3c11286.
[48] S. Kim, D.-Y. Han, G. Song, J. Lee, T. Park, S. Park, Resilient binder network with enhanced ionic conductivity for high-areal-capacity Si-based anodes in Lithium-Ion batteries, Chem. Eng. J. 473 (2023) 145441, https://doi.org/10.1016/j.cej.2023.145441.
[49] S. Nam, Y. Kim, S.H. Kim, H.B. Son, D.-Y. Han, Y.H. Kim, J.H. Cho, J. Park, S. Park, Tailoring three-dimensional cross-linked networks based on water-soluble polymeric materials for stable silicon anode, ACS Appl. Mater. Interfaces 16 (2023) 594–604, https://doi.org/10.1021/acsami.3c13896.
[50] W. Tang, L. Feng, X. Wei, G. Lai, H. Chen, Z. Li, X. Huang, S. Wu, Z. Lin, Three-dimensional crosslinked PAA-TA hybrid binders for long-cycle-life SiO_x anodes in lithium-ion batteries, ACS Appl. Mater. Interfaces 14 (2022) 56910–56918, https://doi.org/10.1021/acsami.2c19344.
[51] Y. He, F. Zhou, Y. Zhang, T. Lv, P.K. Chu, K. Huo, High-toughness and hierarchical stress-dissipating binder based on physicochemical dual-cross-linking for high-performance silicon anodes, ACS Appl. Mater. Interfaces 17 (2025) 21206–21214, https://doi.org/10.1021/acsami.4c22696.
[52] Y. Kang, N. Dong, F. Liu, D. Lin, B. Liu, G. Tian, S. Qi, D. Wu, Constructing high-toughness polyimide binder with robust polarity and ion-conductive mechanisms ensuring long-term operational stability of silicon-based anodes, J. Energy Chem. 93 (2024) 580–591, https://doi.org/10.1016/j.jechem.2024.02.031.
[53] Y. Wang, N. Dong, B. Liu, K. Qi, G. Tian, S. Qi, D. Wu, Enhanced electrochemical performance of the $LiNi_{0.8}Co_{0.1}Mn_{0.1}O_2$ cathode via in-situ nanoscale surface modification with poly (imide-siloxane) binder, Chem. Eng. J. 450 (2022) 137959, https://doi.org/10.1016/j.cej.2022.137959.